J. Wind Eng. Ind. Aerodyn. 133 (2014) 18–26

Contents lists available at ScienceDirect

Journal of Wind Engineering and Industrial Aerodynamics

journal homepage: www.elsevier.com/locate/jweia

Study on the surface pressure distribution of cubes in cross-wind arrays

Hee-Chang Lim [a,*], Kenji Tsukamoto [b], Masaaki Ohba [b], Kunio Mizutani [b]

[a] School of Mechanical Engineering, Pusan National University, San 30, Jangjeon-Dong, Geumjeong-Gu, Busan 609-735, South Korea
[b] Department of Architecture, Faculty of Engineering, Tokyo Institute of Polytechnics, Atsugi, Kanagawa, 243-02/3, Japan

ARTICLE INFO

Article history:
Received 22 December 2013
Received in revised form
11 July 2014
Accepted 17 July 2014
Available online 8 August 2014

Keywords:
Interference effect
Side-by-side cubes
Surface pressure
Effects of the gap
Wind tunnel measurement

ABSTRACT

In this study, effects of the gap on equal-spaced cubical bodies (150 mm × 150 mm × 150 mm) placed in a turbulent boundary layer were investigated inside an atmospheric boundary layer wind tunnel. This study includes various measurements of surface-pressure distribution around a building in close proximity to surrounding obstacles. In addition, we examined the surface-pressure variation with cube distances (G) at 75 mm (0.5 h), 150 mm (1 h), 225 mm (1.5 h) and ∞ (i.e., a single cube). The experiments conducted included some boundary layer wind tunnel tests with Hot Wire Anemometry (HWA) and mean and fluctuating surface-pressure measurements around a set of cubes aligned in parallel. The tunnel tests were carried out at two different Reynolds numbers ($Re = 4.6 \times 10^4$ and 6.7×10^4), based on wind velocity U_h (4.5 m/s and 7.3 m/s) at a cube height h. On analyzing the results, we discovered that the gap effect of surrounding models has a significant influence on the pressure variation around the central model. The overall surface-pressure coefficient around the central structure was generally found to increase as the gap (G) between the structures was increased.

1. Introduction

Over the past decades, the wind load characteristics around bluff bodies have been of fundamental interest in the study of fluid dynamics. In addition, these characteristics have long been considered as a critical design parameter from various engineering points of view civil, fluid mechanical, and architectural. Numerous empirical and simulated data and comparisons of the flow around buildings of all kinds have therefore been carried out. Most of the past studies fall into one of three categories: tandem arrangements, in which one building is directly in the wake of the other; side-by-side arrangements, in which the buildings are arranged transverse to the incoming flow; and staggered arrangements, in which the buildings are arbitrarily configured. The flow field, pressure coefficients, force variation, and intensification or suppression of vortex shedding are highly dependent on the configuration of the building, and on the shape and spacing of the building group due to both wake and proximity-induced interference effects.

A frequently cited paper in this area, especially cylindrical models, Zdravkovich (1977, 1987), described wind-tunnel experiments that measured the flow around two surface-mounted cylinders. In that paper, Zdravkovich analyzed the problem of flow interference that arises when two cylinders are placed side-by-side, in tandem, and in staggered arrangements in steady state. It was observed that the vortex-induced force and the vortex shedding pattern were completely different from those found on a single cube in the case of the same Reynolds number. It was one of the first demonstrations of the crucial importance of modeling appropriately the design details of a building configuration. However, that early work only focused on the importance of ensuring appropriate simulation of the building arrangements.

A number of findings on interference have been obtained even though most of them involve only two bodies in close proximity. The most common interference mechanisms include shelter effect, flow channelling, flow asymmetry, and wake buffeting. When two buildings are in a tandem arrangement, the upstream building generally provides shielding for the downstream building. This normally leads to a reduction in the mean along-wind force on the downstream building. However, fluctuating wind force may become larger due to turbulence buffeting (Bailey and Kwok, 1985). The presence of a neighboring building introduces asymmetry in wind flow pattern around the target building, leading to the possibility of highly magnified wind-induced torsion (Zhang and Kwok, 1994). An upstream building is generally not significantly affected by a downstream building but when two buildings are in very close proximity, wind flow is channelled to sweep through the building gap.

Above all, the study of two bluff bodies placed close together is generally considered to be important due to their interaction effects on each other. Ricciardelli and Vickery (1998) investigated the aerodynamics forces acting on a pair of square cylinders in

* Corresponding author. Tel.: +82 515 102 302; fax: +82 515 125 236.
E-mail address: hclim@pusan.ac.kr (H.-C. Lim).

http://dx.doi.org/10.1016/j.jweia.2014.07.009
0167-6105/

a tandem and in a side-by-side arrangement. It was measured that the pressure in smooth and turbulent flows with angles ranging from 0° to 90° and wide-range separations from 2 H to 13 H. It was observed that for large angles of attack, the highest values of the root mean square (rms) force coefficients were found for large separations. In addition, To and Lam (2003) reported some interesting interference effects not previously observed in past investigations on two buildings in the case of a larger separation. However, with regard to the effect of the gap on groups of buildings, interference effects on a group comprising three or more buildings have not been studied in detail so far, and there are many problems still left to be investigated.

The immediate emphasis in this paper is on a group of cubical bodies with various gaps. The gap between bodies is responsible for the type of wake generated and, ultimately, for the structural loading, pressure, and (especially) structural excitation. For example, with the inclusion of another building in a side-by-side arrangement, the loading pattern becomes quite complex. The buildings may experience increased or reduced wind loads depending on their geometries and spacing, as well as the characteristics of wind flow and upstream terrain. This paper consists of a carefully designed set of experiments on boundary layer flow over surface-mounted side-by-side cubes. These experiments were conducted under various speeds in an atmospheric boundary layer wind tunnel to allow variations in Re, while the upstream boundary layer characteristics were kept relatively similar. Data is also presented with the previous wind-tunnel measurements, yielding a further change in Re and validating the present wind tunnel experiments.

The flow inside a wind tunnel was designed to be similar to the (rural) atmospheric boundary layer. Here, the main emphasis is primarily on the extent to which the flows are affected by Re, and attention is concentrated on the effect of the gap defined by distances between the bodies corresponding to 0.5 h, 1.0 h, 1.5 h and ∞ (i.e., a single cube); where *h* is the height of the cube. This paper is organized as follows. Section 2 outlines wind tunnel details and techniques. Section 3 describes the generation of a simulated turbulent boundary layer and the surface-pressure variation around a single cube. Section 4 describes the surface-pressure variation resulting from gaps in the models, and also presents and discusses the major results. Finally, Section 5 presents the major conclusions.

2. Design of the wind tunnel experiment

2.1. Configuration of the wind tunnel

The wind tunnel tests were conducted in the turbulent boundary layer wind tunnel (Fig. 1) of the Wind Engineering Research Center at Tokyo Polytechnic University (TPU) in Japan. This wind tunnel is an open-circuit, low-speed wind tunnel designed for wind environmental assessment and ventilation studies. Most of the experiments were conducted in the end-part test section of the tunnel, where the sectional dimensions were 1.2 m width, 1.0 m height, and 14 m length, with a maximum wind speed of approximately 30 m/s. However, for reasons of structural stability and safety, the wind tunnel usually operates at a speed lower than rated. Table 1 gives the dimensions of the group of surface roughness blocks used in the wind tunnel to generate the simulated turbulent boundary layer. The details of the generated turbulent boundary layer are illustrated in Fig. 1. The combination of turbulence-generating spires at the entrance and arrays of various rectangular blocks on the tunnel floor is a general way of generating a deep turbulent boundary layer [see Cook, 1973, 1977 in detail].

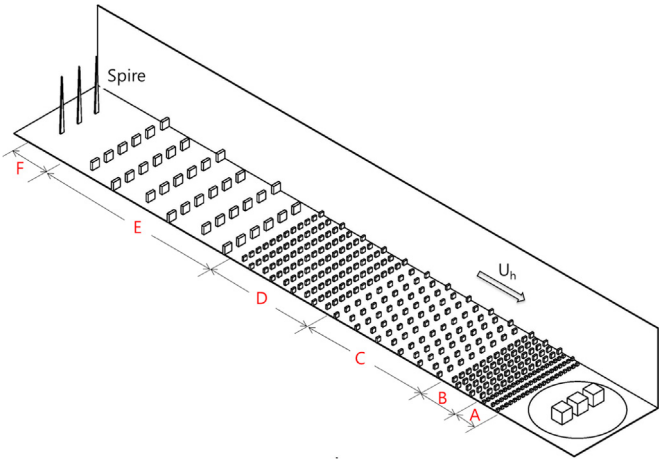

Fig. 1. Schematic diagram of the wind tunnel.

Table 1
Group of surface roughness blocks used in the tunnel.

Configuration	A	B	C	D	E	F
Size [W × H] (mm^2)	30 × 30	50 × 50	50 × 50	50 × 50	98 × 98	70 × 700
No. elements	60	60	128	108	36	3
Length (mm)	240	525	1780	1435	2450	450

2.2. Description of the measurement system

Flow measurements were conducted using hot wire anemometry (in our case, a multi-channel Constant Temperature Anemometry (CTA) module and a split-fiber probe of DANTEC (55H31)), which is highly sensitive to turbulent wind flow. For calibrating this precise measurement system, a well-known, less-sensitive, more-robust calibrator was used with a Pitot tube and pressure-difference manometer (MKS270). Surface pressure variation around the models is also an important indicator of the surrounding characteristics. It was obtained using a multi-channel pressure-measurement system in which each channel is connected to an analogue/digital (A/D) converter in such a way that all 32 channels of surface pressure were directly and simultaneously acquired and transferred to a personal computer for storing the data. The reference static and total pressures were monitored using a Pitot tube located 4 m upstream at a height of 0.5 m above the roof of the model. A multi-channel pressure-measurement system was utilized during the measurement and 65,536 sequential samples of pressure at all the pressure taps were obtained simultaneously at a sampling frequency of 1024 Hz. In order to reduce the effect of the diameter and length of the Teflon® pressure tube (approximately 1 mm and 0.5 m, respectively) (the diameter and length are approximately 1 mm and 0.5 m, respectively), the mean and fluctuating pressures were calibrated before the main measurement. In this case, the calibration was based on the correction of distortion effects caused by tubing systems. In particular, the frequency response of the tubing effect was numerically compensated for frequencies ranging up to 250 Hz using the gain and phase-shift characteristics of the pressure measuring system (Irwin et al., 1979). In addition, the pressure records were digitally low-pass filtered at 300 Hz.

2.3. Cube models and surface-pressure coefficient

As shown in Fig. 2, the models (150 mm in height, 150 mm in width, and 150 mm in length), were all made from 10-mm-thick acrylic. One of them was used to measure the surface pressure and

had many pressure taps all around it. The surface-pressure taps were all of the same size (1.0 mm i.d. and 1.5 mm o.d.) at salient points on top of the roof and at the front, side, and rear surfaces. The pressure taps are located as follows: 85 in total with 20 on the front face, 20 on the side, and 45 on the top. The arrangement of the pressure taps is shown in Fig. 2. Silicone tube connections to a micro-manometer facilitated the measurement of mean surface pressure.

In this study, the pressure taps along the centerlines of the building faces were considered for several reasons. First, the pressure transducer was limited to operating on 32 channels simultaneously. Therefore, the salient points had to be chosen in the earlier stages of the tunnel experiment. More salient points will be included in future studies. Second, the pressure measurement of a single cube was necessary to justify whether current results are consistent with that of well-known prior works. Finally, to our knowledge, pressure measurements of centerlines or face diagonals (not included in the paper) are fundamental tests for practical applications such as wind, architectural, and civil engineering.

The difference between the surface pressure p (on the surface of the cube) and the static pressure p_0, measured at the reference position using a Pitot-static probe upstream of the cube, was non-dimensionalized by using U_h, the velocity at the cube height, to give the classical pressure coefficient C_p. Since the measurement system connected to an analog digital (A/D) converter has 32 stand-alone pressure transducers, the calibration of all these sensors is automatically controlled and simultaneously performed.

2.4. Generation of the deep turbulent boundary layer

All the mean and fluctuating velocity data were normalized using the mean velocity U_h measured at the cube height h (i.e. the velocities were 4.5 and 7.4 m/s, respectively, at a cube height of 150 mm). The mean-velocity profiles obtained at two different

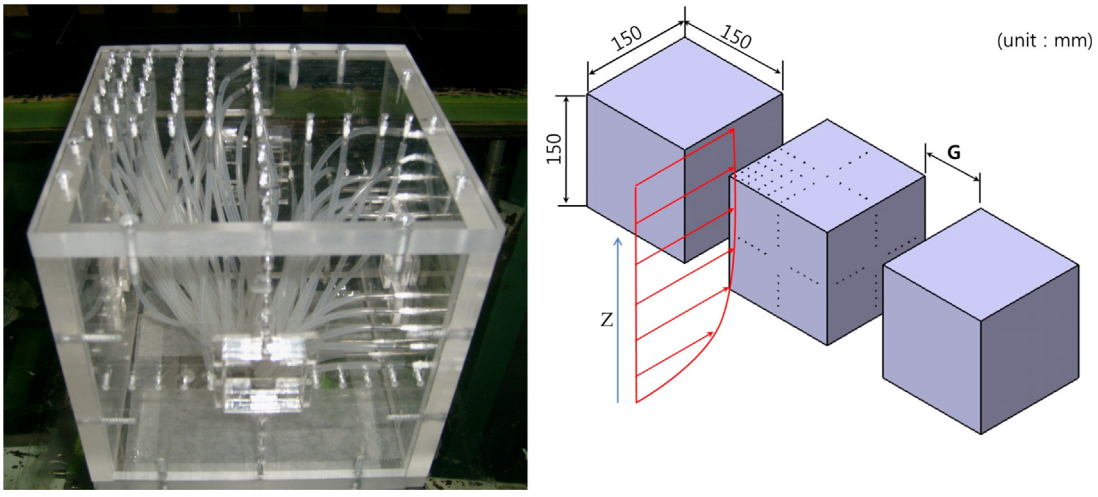

Fig. 2. Cubical model and pressure tapping.

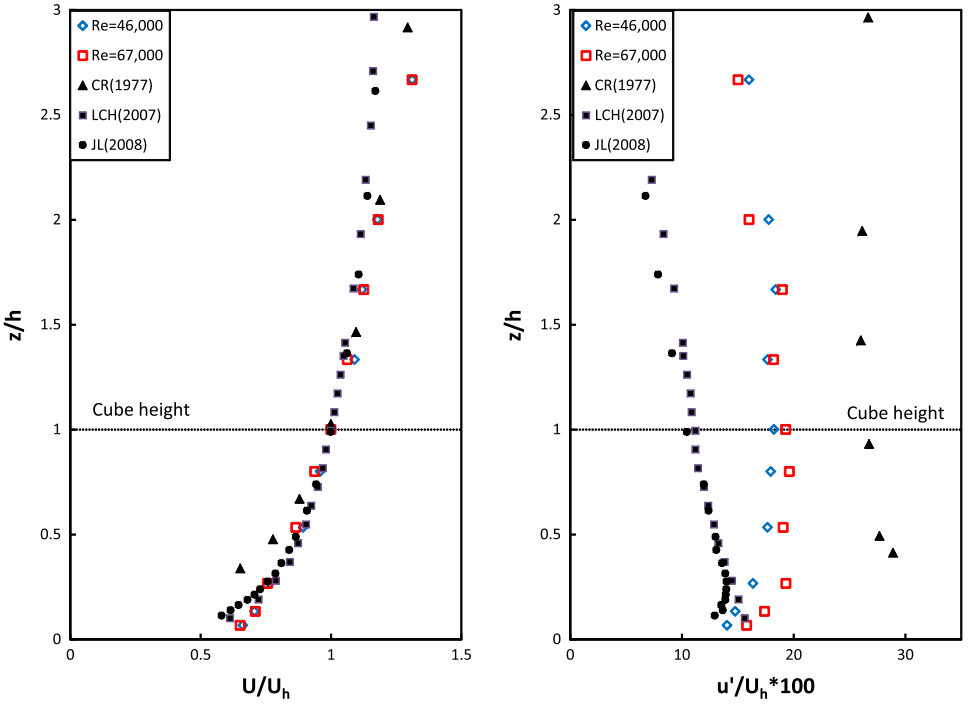

Fig. 3. Mean velocity (a: left) and turbulence intensity profiles (b: right).

wind speeds in the tunnel are illustrated in Fig. 3. Careful consideration was given to selecting turbulent boundary layer generation procedures as close as possible to natural atmospheric mechanisms, in accordance with modern boundary layer wind tunnel techniques. The measurements were made 7.2 m downstream of the vortex spire (point F in Fig. 1) of the wind tunnel. This was done with the aim of ensuring that the simulated flow would eventually become a fully developed shear flow specifically designed to be similar to the (rural) atmospheric boundary layer. In order to confirm the feasibility of the tunnel test data, the data from the boundary layer profiles were compared with the corresponding data from past papers – Castro and Robins (1977) (CR), Lim et al. (2007) (LCH), Jeong and Lim (2008) (JL), and Lim (2009). Note in particular that the velocity ranges (ms^{-1}) imply Reynolds number ($Re = U_h h/v$) variations of $4.6 \times 10^4 \le Re \le 6.7 \times 10^4$ (i.e., 3.0×10^4 in CR, 7.3×10^4 in LCH, and 4.6×10^4 in JL and Lim) in the tunnel, and that the overall comparison shows little difference between the values. Similar mean velocity profiles were achieved with little differences while the upstream condition was maintained, as described previously. However, the turbulence intensity tends to differ depending on the roughness of the floor. The results of this study (i.e. $Re = 4.6 \times 10^4$ and 6.7×10^4) were similar to each other but difficult to compare with other past results, as shown in Fig. 3(b). Fig. 3(b) shows turbulence intensity ($u'/U_h \times 100$) versus the non-dimensionalized height (z/h) in terms of the characteristic length and velocity. Note here that the characteristic length is the cube height, and the characteristic velocity is the mean velocity at the cube height. Interestingly, the mean velocity profiles at cube height were almost identical, whereas those of the turbulence intensity were substantially different depending on the upstream surface condition, i.e., the dimensions of the floor patch of the wind tunnel. As shown in Fig. 3(b), the discrepancy of turbulence intensity is approximately a factor of three. It should also be noted that the surface pressure on the cube would be changed depending on the different characteristics of the mean and fluctuating flow, and a three times higher fluctuating flow would be a precursor to explaining the different pressure distributions among them in due course. Note here that Daniels et al. (2013) reported detailed surface-pressure distributions of a CAARC standard tall model building depending on the integral length scale and turbulence intensity. In the figure, the turbulence intensity in the current study is 18.2% and 19.2%, whereas for CR it was 26.7%, while LCH and Lim were 11.2% and 12%, respectively.

Fig. 4 shows the longitudinal-velocity spectra, $E_u(f)$, obtained at $z=h$. The kinetic energy in the turbulent boundary layer is drawn out of the mean flow by instabilities of a relatively large scale, and this energy is dissipated into heat by numerous eddies of very small size. The energy-containing eddies in atmospheric surface boundary layer turbulence are typically of a scale that is of the order of the mixing length. Therefore, turbulence energy must flow from large scales to relatively small scales in order for dissipation to take place. In fact, no exact theory exists for this mechanism, and thus no general theory exists for the overall spectral shape. However, for the intermediate range between the two scales, the spectra must obey a power law in wavenumber with a power index of $(-5/3)$. In particular, Fig. 4(a) indicates the collapse of the slope (5/3) in the inertial subrange as expected. In addition, Fig. 4(b) shows the non-dimensionalized spectrum of the length scale compared with the ESDU spectrum (ESDU Report, 1993). As shown in the figure, the integral length scale normalized by $z=h$ is about $L_x/h = 3.3$.

3. Turbulent boundary layer and surface pressure around a single cube

3.1. Surface-pressure distribution of a cubical model (1×1)

One of the priorities of this study was the validation of the surface pressure around a cubical model. To achieve this, pressure measurements and precise analysis were carried out on the base of the non-dimensional parameter C_p. Regarding the blockage effect of the models in the wind tunnel, cross-section blockage ratios (BRs) were 1.9% (single cube) and 5.6% (three parallel-aligned cubes). (In the case of speed-up around the obstacle, the effect scales with the ratio of the area of the obstacles cross-section to that of the frontal cross-section of the domain.) Maskell (1963) addressed problems with non-streamline flow bodies, such as bluff-body testing in a closed-wall wind tunnel and partially stalled shapes such as cubical/rectangular bodies. The Maskells theory holds for a close-axis symmetric wake in 3D flows. The correction of the dynamic pressure ratio is as follows:

$$\frac{q_c}{q} = \left[1 + \frac{5}{2} C_D \left(\frac{S}{C}\right)\right] \quad (1)$$

where q_c is corrected dynamic pressure, q is uncorrected dynamic pressure, S is the maximum cross-sectional area of the body, C is the cross sectional area of the tunnel, and C_D is uncorrected wind-axis drag coefficient ($\approx$1.0). The profiles of surface pressure coefficients in Figs. 5–7 are all corrected by using Eq. (1) so that the pressure distributions deserve to be highly reliable.

Fig. 5 depicts the variation of the mean surface pressure C_p along the axial centreline of the cube obtained in the wind tunnel.

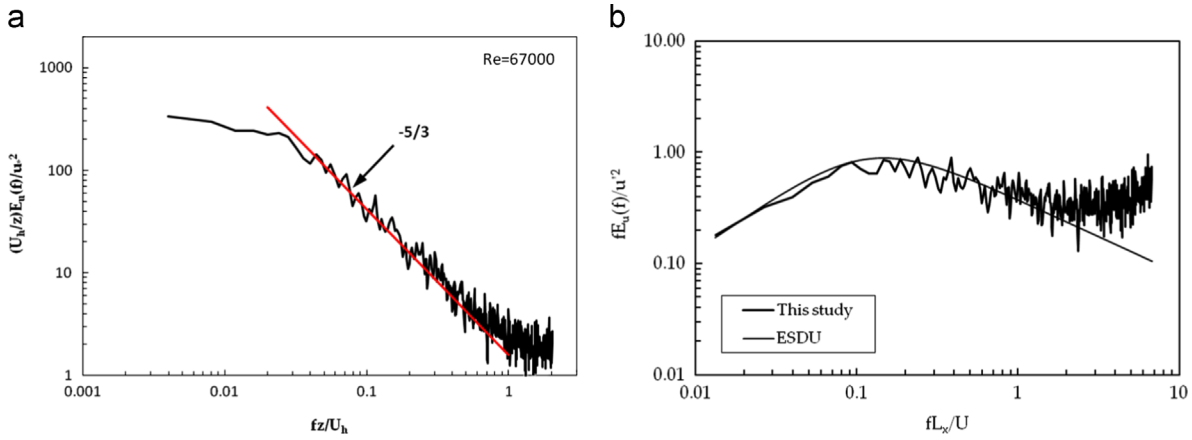

Fig. 4. Spectra of the axial turbulence component at $z=h$; (a) normalized by u_*^2; (b) normalized by u'^2.

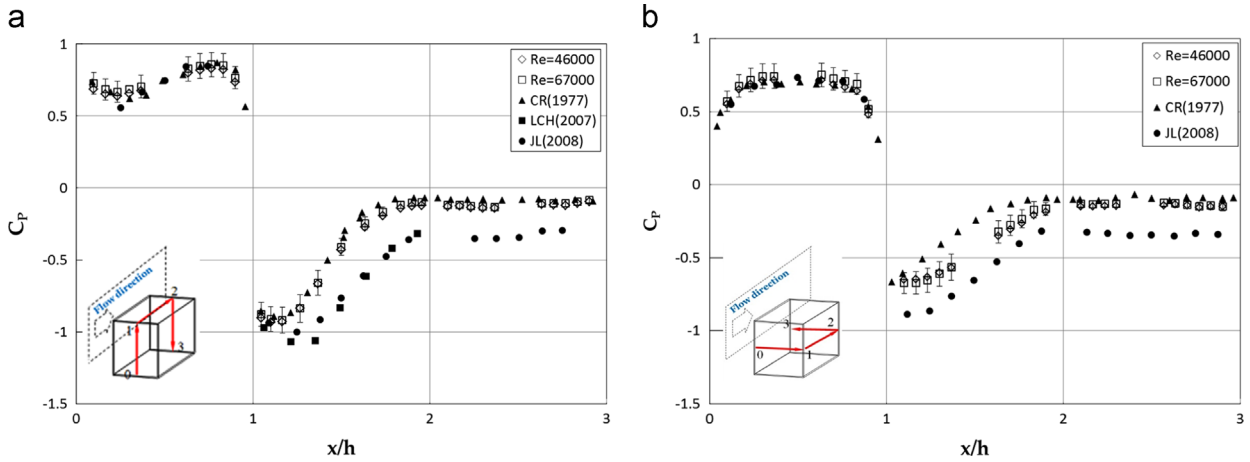

Fig. 5. Mean surface static pressure along the central section (a: left) and along the mid-height (b: right) of the cube with wind normal to the face; the current experiments are shown by mean values and error bars.

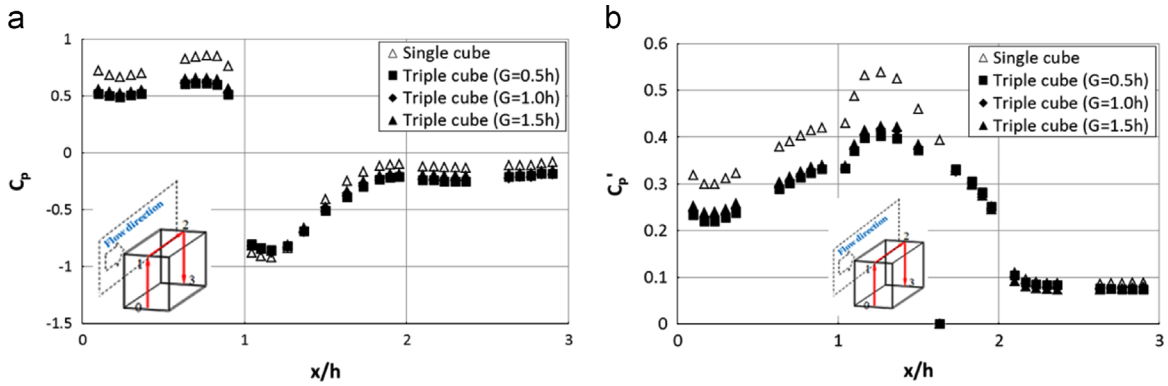

Fig. 6. Mean (a: left) and fluctuating (b: right) surface pressure along the centreline of cube with wind normal to face.

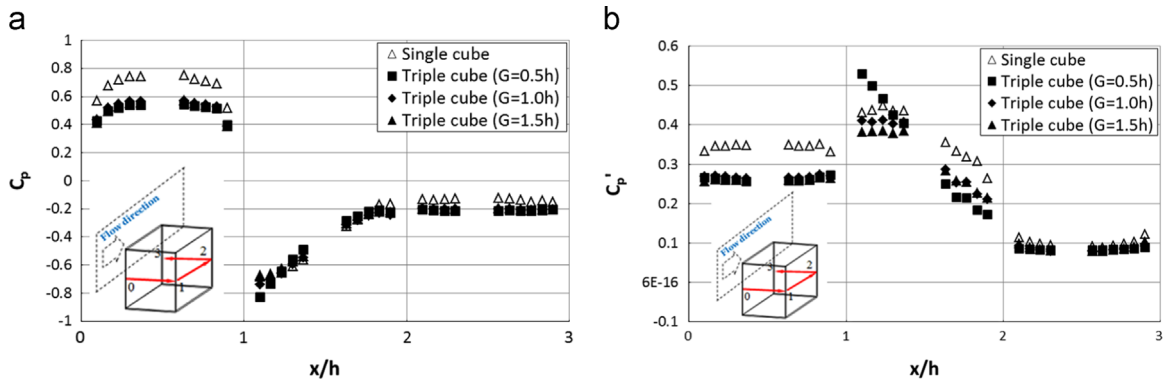

Fig. 7. Mean surface static pressure (a: left) and fluctuating pressure (b: right) at the mid-height of cube.

It also graphically compares current results to those obtained by others in past studies. In addition, an uncertainty analysis was conducted to find the error in the experimental data. It was carried out for all experimental results to determine a confidence level, following the method suggested by Coleman (1989). The total error incorporates both bias error and precision error. The bias error was minimized with careful calibration of measuring instruments. To evaluate the precision error, the standard deviation S_u of five sample records was calculated for the surface pressure data from each set. The value of the t-distribution for 95% confidence and five samples was 2.776. The total error with 95% confidence is depicted as error bars.

Fig. 5(a) depicts the variation of the mean surface pressure C_p along the axial centreline of the cube obtained in the wind tunnel. The typical regime of pressure distribution on the top surface was as expected: the largest negative-surface-pressure region was on the upper corner of the leading edge. However, the substantial pressure recovery associated with the attachment process was just beyond separation, as past studies (e.g., Castro and Robins, 1977; Lim et al., 2007) have frequently shown. As shown in the figure, the current surface-pressure profile is reasonably located in the middle of the others, which means that the turbulence intensity and other inflow conditions are slightly different so that it can be easily conjectured that the surface-pressure distribution around

the cube could be different based on the inflow boundary condition. For example, the result of CR was obtained under a specific inlet flow condition of high turbulence intensity, whereas LCH was obtained under relatively lower turbulence intensity (Castro and Robins, 1977; Lim et al., 2007; Lim, 2009).

Fig. 5(b) shows the mean surface-pressure profile along the mid-height of the cube. Interestingly, the pressure coefficient of the side surface was relatively different but was consistent when compared with the result on the top surface of Fig. 5(a). The figure shows that the surface pressure variation is highly dependent on the upcoming turbulence intensity, with a relatively smaller dependence on the mean velocity. For instance, compared with the turbulence intensity at the mid-height location of the cube (i.e., $z/h=0.5$ in Fig. 3(b)), the upstream turbulence intensity (i.e. see solid triangles) of CR is almost 30% whereas the value of JL is around 10%. LCH observed that the upstream turbulence reduced the surface pressure around the cube i.e. at the top surface and mid-height in our case. In the other example, the results (i.e. see solid circles) of JL in the figure obviously show a consistent trend. In the other example, the result (i.e., see the symbols of solid circle) of JL in the figure obviously shows the consistent trend. With regard to the Reynolds effects arising from the past issue, the current data (i.e. see hollow diamonds and hollow squares) in both figures imply that the velocity and size have no effect on the Reynolds number. Note that the differences in the turbulence intensity profiles are due to the different scales of roughness. Therefore, given that the surface pressure profile around a cube is appropriate for understanding the flow structure, these results can act as the basis for the rest of the pressure profiles. The next section discusses the surface pressure profiles around the side-by-side cube with various gaps under the same turbulent boundary layers.

4. Surface-pressure variations with gaps in the models

4.1. Effect of the gap on the mean and fluctuating pressure

Fig. 6 shows the mean and fluctuating surface pressure along the centreline of a cube among the side-by-side cubical models with various gaps at 0.5 h, 1.0 h, 1.5 h, and ∞ (i.e., a single cube), where h is the height of the cube. In Fig. 6(a), the single cube and the triple cube both have fairly expected tendencies in the overall region. In the case of the front face, C_p for the triple cube is generally lower than that for the single cube (approximately 0.1). This may have been caused by the 2-dimensional flow regarding the triple cube as one long, longitudinal block by placing more blocks on both sides of a single cube. On the top surface, however, a separation occurs in the leading edge of the cube and the separation points seem to have similar surface coefficients in the leading edge. However, as the flow travels further downstream, the single cube recovers faster than the triple cube.

Fig. 6(b) shows a typical fluctuating pressure distribution along the centreline of the cube among the side-by-side cube models. It has a substantial surface fluctuation peak in the leading edge region of the top surface, making the maximum rms approximately 0.55. Interestingly, the fluctuating pressure of the single cube is generally higher than that of the triple cube. This increased fluctuating pressure might be caused by the flow interference effect on the central cube coming from a result of the separated flow on the leading and side edges.

Fig. 7 shows the mean and fluctuating surface pressure at the mid-height of the cube, with various gaps at 0.5 h, 1.0 h, 1.5 h and ∞. In Fig. 7(a), although the regions at the front and rear faces show some deviations, the overall features of the mean surface pressure are very similar to the result of Fig. 6(a). In the region of $x/h=1.1$–1.2, there are pressure variations against the gap, which has a peak, especially around the leading edge (or corner) around -0.95 when $G=0.5$ h and reduces to approximately 0.75 for the single cube and triple cube when $G=1.5$ h. These facts may highlight the interference effects of the adjacent bodies. The interference effects are more dominant on the fluctuating surface pressure at the mid-height of the cube. As shown in Fig. 7(b), the peak fluctuating pressure at the leading edge does not appear in the single cube, but there is a peak for the triple cube for $G=0.5$ h. It is easily seen that the fluctuating pressure varies widely depending on the gap between the bluff bodies, which is not observed in the surface-pressure results along the centreline of the bodies.

The spectral content of the fluctuating-surface-pressure distribution is worth some consideration. Detailed pressure spectra were not obtained for all surface locations and wind orientations, but Fig. 8 shows the spectra obtained near the central point on the top of the cube surface. In this figure, a small secondary hump occurs at around $fh/U_h \approx 0.6$. LCH observed this as a typical in-phase shedding, which is usually observed in strongly three-dimensional flows around a surface-mounted body. However, this secondary hump increases on the side surface at around $fh/U_h \approx 0.8$, and the peak of this hump is higher than the side surface of the single cube. This could be caused by the gap flow between the cubes, which seems to squeeze and make the shedding events faster. Further comments regarding Fig. 8(b) are appropriate. The sampling frequency for the pressure measurements was high enough to return the expected (highest frequency) f^{-5} range before considering filtering or aliasing effects. However, highest-frequency range of the longitudinal velocity was not as broad, but likely would have been if higher sampling rates had been used. In addition, regarding the second hump, we are not entirely confident of this result, so we did not describe this phenomenon in detail, but we did obtain proper pressure signals. These were measured at a 1 kHz sampling rate with a 400 Hz low pass filter. In fact, the frequency range of the second hump is

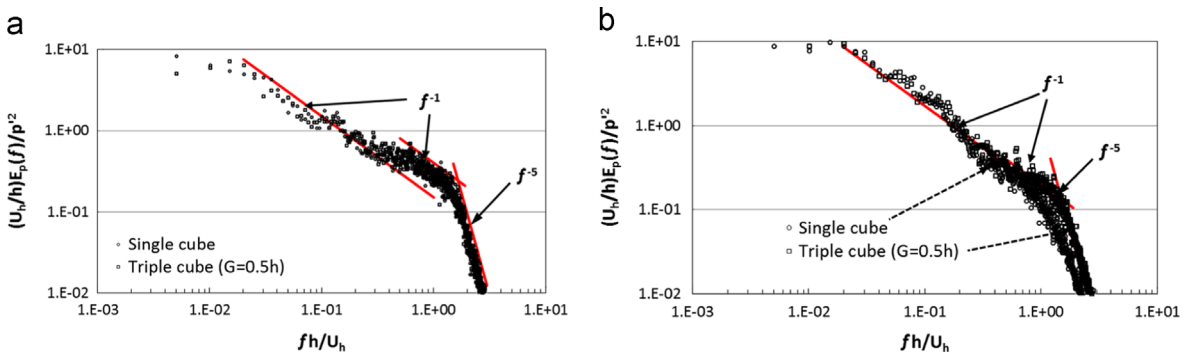

Fig. 8. Surface pressure spectra measured near central point (a: left) on cube top surface and (b: right) on side to emphasize behavior in high and medium frequency range.

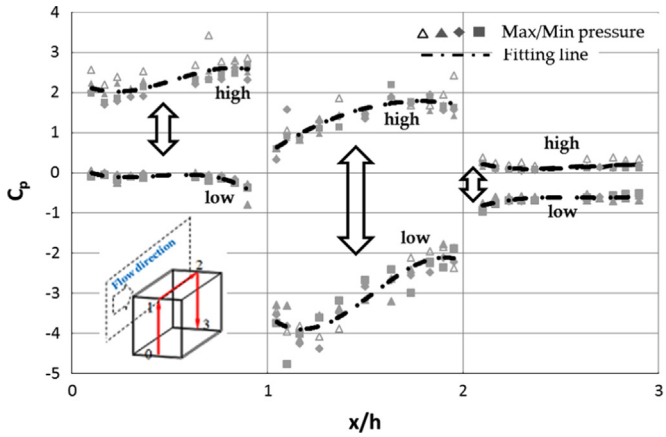

Fig. 9. Maximum and minimum surface pressure along the centreline of cube with various gap (△: single cube, ▲: triple cube (G=0.5 h), ◆: triple cube (G=1.0 h), ■: triple cube (G=1.5 h)).

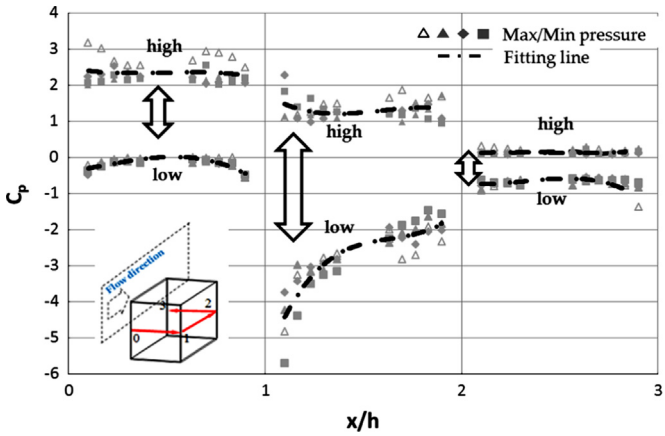

Fig. 10. Same as Fig. 9 but at the mid-height of cube.

Table 2
Empirical constants used in the polynomial equation of Fig. 9.

Centreline	Face	a	b	c	d
Maximum	Front	−5.5	8.7	−3.1	2.3
	Top	−0.2	−1.4	6.4	−4.4
	Rear	−1.6	12.7	−33.1	28.6
Minimum	Front	−4.8	6.3	−2.4	0.2
	Top	−9.2	42.3	−61.5	24.8
	Rear	2.0	−15.5	40.0	−35.0

Table 3
Empirical constants used in the polynomial equation of Fig. 10.

Centreline	Face	a	b	c	d
Maximum	Front	−1.8	2.7	−1.2	2.5
	Side	−4.1	19.7	−30.6	16.8
	Rear	0.8	−5.5	13.3	−10.5
Minimum	Front	−2.4	1.1	0.8	−0.4
	Side	11.3	−55.6	91.8	−53.2
	Rear	−4.0	28.3	−65.6	49.6

distributed so broadly between 30 Hz and 60 Hz that it could be due to the electric power source. We will pursue this issue further in the future.

4.2. Effects of the gap on the maximum and minimum surface pressure

Fig. 9 shows the maximum and minimum surface pressure along the centreline of the cube, with various gaps at 0.5 h, 1.0 h, 1.5 h and ∞. In Fig. 9, the results of each maximum and minimum pressure distribution are close together and not distinguishable from each other, and they are plotted for a curve to fit with all points. In addition, the symbols, the maximum and minimum pressure variation, all fit well with each dashed line of a cubic polynomial equation ($y=a+bx+cx^2+dx^3$, where a, b, c, and d are all constants as shown in Table 2) in each face (i.e., front, top, and rear faces).

Fig. 10 shows the maximum and minimum surface pressure at the mid-height of the cube, with various gaps at 0.5 h, 1.0 h, 1.5 h, and ∞. Table 3 denotes the empirical constants used in the figure. It is not easy to determine if there are the effect of the gap on the overall region around the cube, i.e., the overall variations in the surface pressure were substantial (i.e. see the range of maximum and minimum pressures), but the effect of the gap was not clearly observed (i.e., see the different symbols, hollow triangle: △, solid triangle: ▲, diamond: ◆, square: ■). However, interestingly, there is a dominant negative peak in some regions around $x/h=1.1$–1.2 on the side face. In Fig. 10(a), there was one point of minimum surface pressures reaching approximately 5.7 at the mid-height of the cube, which is not observed on the other faces and is definitely caused by the gap flow (i.e., effect of the gap). Therefore, in these regards, if it is necessary to consider a structural design with adjacent structures, one should understand the minimum surface pressure as well as the maximum wind gust.

4.3. Overall analysis of the effect of the gap

Figs. 11–13 show the mean and fluctuating surface pressures at several points on the front face, top face, and rear face of the cube with various gaps at 0.5 h, 1.0 h, and 1.5 h; h is the height of the cube. As shown in the figure, the surface pressure coefficient tends to increase as a polynomial function depending on the gap G, except for the rear face of the cube. In the case of G=3 (the result from a single cube), the points must be located in the wind-tunnel test section where the effect of the gap between multiple cubes is experienced. The interesting fact is that while the single cube is chosen as a reference of gap G=3 accidentally, it reasonably well matches well with the fitting curves, which was never been achieved before. Note that the dotted and solid lines are fitting curves and are suitable for identifying the proper place to understand the interference effect of multiple cubes. The regression curves used in Figs. 11–13 are assumed to be a polynomial shape defined by

$$C_p = p + q \times G^n \tag{2}$$

where p is the intersection point on the y-axis, q is the constant coefficient (in this study, q is in the range 0.01 to 0.02), and the power exponent n is an arbitrary constant. For the simple approach, the exponent n is set to 2 (see Table 4).

As shown in Fig. 11, the gap G is the primary factor in increasing the surface pressure coefficient. From these results, a narrow gap between the bodies seems to increase the speed of the valley flow resulting in a higher speed and lower pressure region whereas a wide gap tends to be a single cube, so it causes the speed to decrease and pressure to increase. It is highly notable that the gap does not affect the surface pressure in the range $G>3$, so this can be regarded to be the equivalent condition of a single cube. Given that the curves fit properly, the overall prediction should be

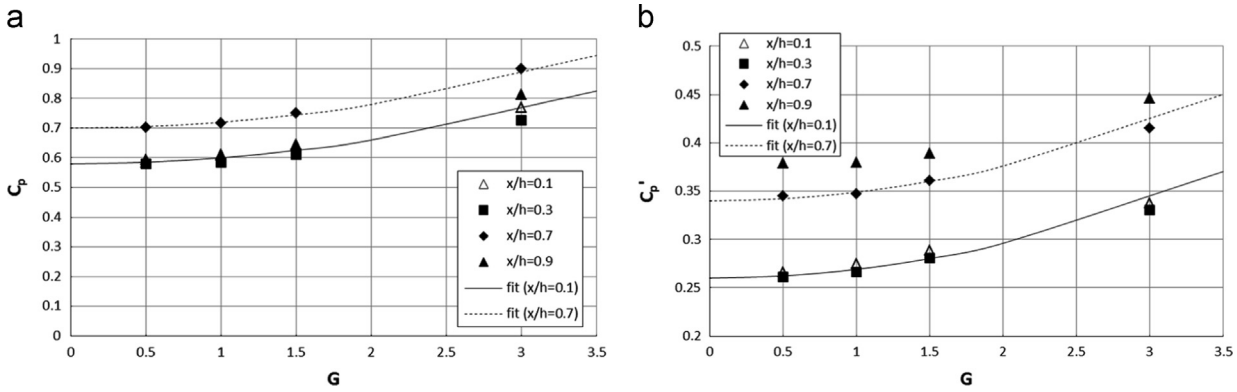

Fig. 11. Mean (a) and fluctuating surface pressure (b) variation on the front face (x/h=0–1) along the central line of cube.

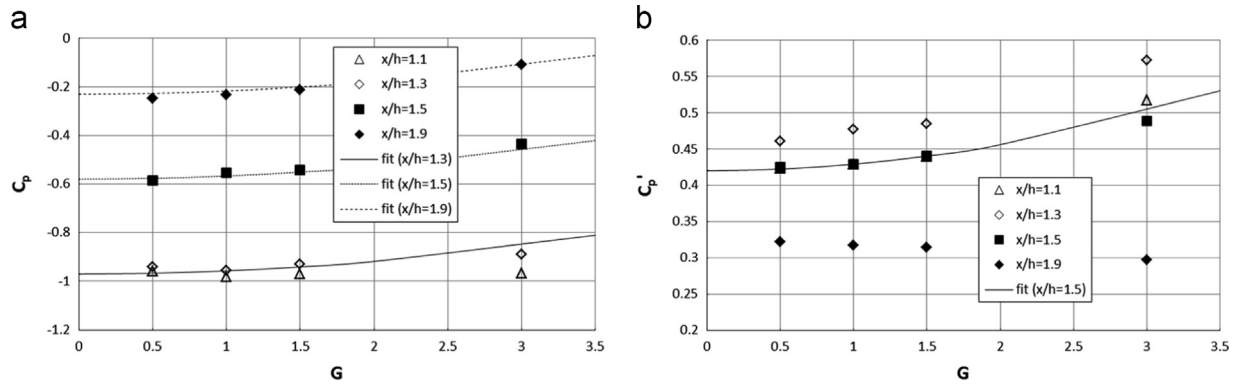

Fig. 12. Same as Fig. 11, but on the top face (x/h = 1–2).

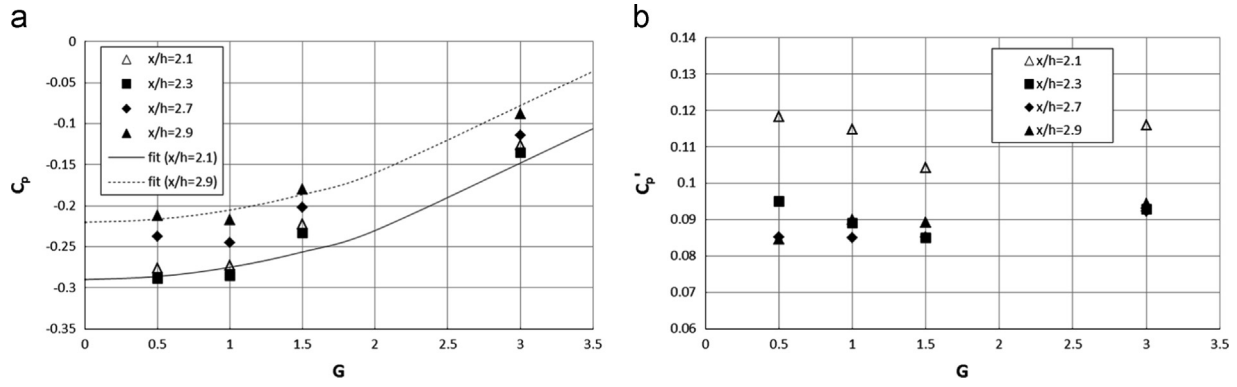

Fig. 13. Same as Fig. 11, but on the rear face (x/h = 2–3).

Table 4
Empirical constants used in the polynomial equation of Figs. 11–13.

Coefficient	Front face (Fig. 11)		Top face (Fig. 12)			Rear face (Fig. 13)	
	$x/h=0.1$	$x/h=0.7$	$x/h=1.3$	$x/h=1.5$	$x/h=1.9$	$x/h=2.1$	$x/h=2.9$
p	0.58	0.70	−0.97	−0.58	−0.23	−0.29	−0.22
q	0.02	0.02	0.013	0.013	0.013	0.015	0.015
n	2						

suitable for the other faces. However, this approach was not valid, as shown in Figs. 12 and 13.

Fig. 12 shows the surface pressure coefficient at several points along the centreline of the top face of the cube with various gaps. Note that the gap G has an effect on the surface pressure along the centreline. The fluctuating pressure is also affected by the gap in the leading edge region but, as it goes downstream, the pressure decreases. In the range $x/h > 1.5$ (i.e. the second half-line on the top surface), in particular, the regression curve of the average pressure appears to be slightly different. This was a crucial point in establishing the proper criteria for designing durable building envelopes. It was also necessary to incorporate the effects of flow

separation and reattachment on the pressure variation of a surface, which are fundamental concepts in the field of wind engineering.

Fig. 13 shows the mean and fluctuating surface pressures at several points on the rear face of the cube. Similar to that outlined above, the mean surface pressure recovered and increased as the gap G increased. On the other hand, the fluctuating surface pressure initially decreased. However, the prediction of the polynomial relation did not work properly on the rear face or even in a reverse direction. This seems to indicate that the rear face is dominated by a highly turbulent region separate from the leading edge of the cube. In addition, this is believed to be not an experiment error but some kind of statistical problem such as the number of sampling data and the bin size used for averaging. However, further analysis with more measurements in the wind tunnel may be needed for better understanding the velocity and surface pressure fields.

5. Conclusion

This study undertook the measurement of surface-pressure distribution around a building in close proximity to surrounding obstacles, with the aim of understanding the surface-pressure variation when the model distance is changed – that is, at 75 mm (0.5 h), 150 mm (1 h), 225 mm (1.5 h) and ∞ (i.e., a single cube). Considerable effort was invested in the performing measurements in the tunnel and validating the results for the surface pressure around the cubical models. From the preceding discussions, the following conclusions can be drawn:

1. In the surface-pressure measurement of a single cube, it has been confirmed that the results of our tunnel test are consistent with those from past papers: Castro and Robins (1977), Lim et al. (2007), and Lim (2009). That is, in terms of the mean upstream velocity, an overall comparison showed no significant difference and the Reynolds number effect was practically negligible.
2. With the central cube among triple cubes, the surface pressure along the central line is considerably less than that of a single cube. However, as the gap between the cubes increases, the surface pressure also increases, approaching that of a single cube.
3. The fluctuating pressure around a single cube is much higher than that of the triple cube arrangement, which means that the flow instability passing over a single cube creates a high fluctuating flow in front of, and on top of, the cube. On the contrary, the fluctuating pressure at the mid-height of the cube has a peak around -0.95 when $G=0.5$ h, which highlights the dominant interference effects of the adjacent bodies on the side surfaces of a cube.
4. Regarding the polynomial equation (i.e. an empirical relationship), the coefficient of surface pressure seems to hold with G^2 in the range of at least $G \leq 3$. However, even though the relation between the gap, G^2, and C_p seems to hold and work, further investigation is required for $G > 3$ at least, where there is a lack of measurement data because of the limitation of the wind tunnel size.

This study includes some crucial points for designing single and multiple structures, in setting up the proper criteria for designing durable building envelopes and in understanding the effects of flow separation and reattachment on the pressure variation of a surface. Even though this study focuses on the gap effect, it requires further investigation for $G > 3$ at least, where there is a lack of measurement data because of the limitation of the wind tunnel size. In the near future, the authors will work further on this empirical relationship to conduct a complementary test and obtain a higher reliability for the interference effect of multiple cubes. Consequently, the authors wish that all of the measurement data would be provided as a reference and fundamental material in the field of wind engineering.

Acknowledgments

This work was supported by the Human Resources Development of the Korea Institute of Energy Technology Evaluation and Planning (KETEP) grant funded by the Korea government Ministry of Knowledge Economy (No. 20114010203080). In addition, this research was supported by Basic Science Research Program through the National Research Foundation of Korea (NRF) funded by the Ministry of Education, Science and Technology (2013005347).

References

Bailey, P.A., Kwok, K.C.S., 1985. Interference excitation of twin tall buildings. J. Wind Eng. Ind. Aerodyn. 21, 323–338.
Castro, I.P., Robins, A.G., 1977. The flow around a surface mounted cube in uniform and turbulent streams. J. Fluid Mech. 79, 307–335.
Coleman, H.W., 1989. Experimentation and Uncertainty Analysis for Engineers. Wiley, New York.
Cook, N.J., 1973. On simulating the lower third of the urban adiabatic boundary layer in a wind tunnel. Atmos. Environ. 7, 691–705.
Cook, N.J., 1977. Wind tunnel simulation of the adiabatic atmospheric boundary layer by roughness barrier and mixing device methods. J. Wind Eng. Ind. Aerodyn. 3, 157–176.
Daniels, S.J., Castro, I.P., Xie, Z.T., 2013. Peak loading and surface pressure fluctuations of a tall model building. J. Wind Eng. Ind. Aerodyn. 120, 19–28.
ESDU Report, 1993. Characteristics of Atmospheric Turbulence Near the Ground, Part: Single Point Data for Strong Winds (Neutral Atmosphere), ESDU-Report No. 85020.
Irwin, H.P.A.H., Cooper, K.R., Girard, R., 1979. Correction of distortion effects caused by tubing systems in measurements of fluctuating pressures. J. Wind Eng. Ind. Aerodyn. 5, 93–107.
Jeong, T.Y., Lim, H.C., 2008. Study on the generation of turbulent boundary layer in wind tunnel and the effect of aspect ratio of a rectangular obstacle. J. Mech. Sci. Technol. 32, 791–799.
Lim, H.C., 2009. Wind flow around rectangular obstacles with aspect ratio. Wind Struct. 12, 299–312.
Lim, H.C., Castro, I.P., Hoxey, R.P., 2007. Bluff bodies in deep turbulent boundary layer: Reynolds number Issues. J. Fluid Mech. 571, 97–118.
Maskell, E.C., 1963. A theory of the blockage effects on bluff bodies and stalled wings in a closed wind tunnel, ARC R&M 3400.
Ricciardelli, F., Vickery, B.J., 1998. The aerodynamic characteristics of twin column. Wind Struct. 1, 225–241.
To, A.P., Lam, K.M., 2003. Wind-induced interference effects on a group of buildings. In: 11th International Conference on Wind Engineering Texas Tech University Lubbock TX, vol. 1, pp. 2405–2410.
Zdravkovich, M.M., 1977. Review of flow interference between two circular cylinder in various arrangements. ASME J. Fluid Eng. 99, 618–633.
Zdravkovich, M.M., 1987. The effects of interference between circular cylinders in cross flow. J. Fluid Struct. 1, 239–261.
Zhang, W.J., Kwok, K.C.S., 1994. Aeroelastic torsional behavior of tall buildings in wakes. J. Wind Eng. Ind. Aerodyn. 51, 229–248.